Electromagnetic wave propagation in the surface-ionosphere cavity of Venus

Fernando Simões, Michel Hamelin, R. Grard, K.L. Aplin, Christian Béghin, Jean-Jacques Berthelier, B.P. Besser, J.-P. Lebreton, J.J. López-Moreno, G.J. Molina-Cuberos, et al.

Electromagnetic wave propagation in the surface-ionosphere cavity of Venus

F. Simões,[1] M. Hamelin,[1] R. Grard,[2] K. L. Aplin,[3] C. Béghin,[4] J.-J. Berthelier,[1] B. P. Besser,[5] J.-P. Lebreton,[2] J. J. López-Moreno,[6] G. J. Molina-Cuberos,[7] K. Schwingenschuh,[5] and T. Tokano[8]

Received 21 November 2007; revised 12 February 2008; accepted 21 March 2008; published 17 July 2008.

[1] The propagation of extremely low frequency (ELF) waves in the Earth surface-ionosphere cavity and the properties of the related Schumann resonances have been extensively studied in order to explain their relation with atmospheric electric phenomena. A similar approach can be used to understand the electric environment of Venus and, more importantly, search for the evidence of possible atmospheric lightning activity, which remains a controversial issue. We revisit the available models for ELF propagation in the cavity of Venus, recapitulate the similarities and differences with other planets, and present a full wave propagation finite element model with improved parameterization. The new model introduces corrections for refraction phenomena in the atmosphere; it takes into account the day-night asymmetry of the cavity and calculates the resulting eigenfrequency line splitting. The analytical and numerical approaches are validated against the very low frequency electric field data collected by Venera 11 and 12 during their descents through the atmosphere of Venus. Instrumentation suitable for the measurement of ELF waves in planetary atmospheres is briefly addressed.

Citation: Simões, F., et al. (2008), Electromagnetic wave propagation in the surface-ionosphere cavity of Venus, *J. Geophys. Res.*, *113*, E07007, doi:10.1029/2007JE003045.

1. Introduction

[2] The propagation of extremely low frequency (ELF) electromagnetic waves in the cavity bounded by two, highly conductive, concentric, spherical shells, like that approximated by the surface and the ionosphere of Earth, was first studied theoretically by *Schumann* [1952]; this phenomenon was first observed by *Balser and Wagner* [1960]. These and other early works have been reviewed by *Besser* [2007]. When electromagnetic sources pump energy in a spherical cavity, a resonant state develops whenever the average cavity perimeter approaches an integral multiple of the signal wavelength. This phenomenon is usually known as the Schumann resonance; it provides information about lightning activity and acts as a "global tropical thermometer" [*Williams*, 1992]. Additionally, Schumann resonances can be used to monitor the tropospheric water vapor concentration on Earth [*Price*, 2000] and assess the global water content of the gaseous envelopes of the giant planets [*Simões et al.*, 2008].

[3] In spite of similarities, the electric environment of Venus is very different from that of Earth; still, the same approach can be applied to the study of ELF wave propagation. Several models of Venus cavity have been proposed [*Nickolaenko and Rabinovich*, 1982; *Pechony and Price*, 2004; *Yang et al.*, 2006; *Simões et al.*, 2008]. However, the characterization of the Schumann resonance in the cavity of Venus is not straightforward because the low-altitude electron density profile and the surface dielectric properties are not known.

[4] Compared to Earth, the surface conductivity is expected to be lower, the days last longer, the planet lacks a significant intrinsic magnetic field, the atmospheric pressure on the surface is much larger, and clouds stretch to higher altitudes. For example, whereas the surface of the Earth is generally assumed to be a perfect electric conductor (PEC) because of its high conductivity, the soil of Venus is dry, which entails important subsurface losses. Unlike Earth's cavity, where the vacuum permittivity approximation is applicable, the atmosphere of Venus is so dense that refraction phenomena affect wave propagation.

[5] The Schumann resonance phenomenon has only been positively identified on Earth. In situ measurements performed on Titan during the descent of the Huygens Probe are still under active investigation, which should confirm whether an ELF resonance has been observed or not [*Simões*, 2007; *Simões et al.*, 2007; *Béghin et al.*, 2007].

[1] CETP, IPSL, CNRS, Saint Maur, France.
[2] Research and Scientific Support Department, ESA-ESTEC, Noordwijk, Netherlands.
[3] Space Science and Technology Department, Rutherford Appleton Laboratory, Chilton, UK.
[4] LPCE, CNRS, Orléans, France.
[5] Space Research Institute, Austrian Academy of Sciences, Graz, Austria.
[6] Instituto de Astrofisica de Andalucia IAA-CSIC, Granada, Spain.
[7] Applied Electromagnetic Group, Department of Physics, University of Murcia, Murcia, Spain.
[8] Institut für Geophysik und Meteorologie, Universität zu Köln, Albertus-Magnus-Platz, Köln, Germany.

0148-0227/08/2007JE003045

Schumann resonances could confirm the possible existence of lightning in the cavity of Venus, which continues to be a controversial issue [*Strangeway*, 2004]. Radio wave observations that had been interpreted as being due to lightning [*Ksanfomaliti*, 1979; *Russell*, 1991, 1993] have not been widely confirmed by measurements in the visible spectrum, though two optical observations are claimed – one performed onboard Venera 9 [*Krasnopol'sky*, 1980] and another with a terrestrial telescope [*Hansell et al.*, 1995]. Similar radio waves detected by Galileo and Cassini were given different interpretations [*Gurnett at al.*, 1991, 2001]. In a recent analysis of Venus Express results, *Russell et al.* [2007] apparently solve the dispute; they have found evidences of lightning on Venus inferred from whistler mode waves in the ionosphere. Nevertheless, the study of ELF wave propagation in the cavity of Venus can provide an independent strategy for the detection and characterization of lightning activity there. For example, *Price et al.* [2007] review several Schumann resonance measurements in the Earth's cavity that are useful to characterize lightning related phenomena, including spatial and temporal variations in global lightning activity, transient luminous events, and planetary electricity.

[6] The novelty of our cavity model includes (1) eigenfrequency corrections due to surface losses; (2) prediction of significant eigenfrequencies line splitting caused by cavity asymmetry; (3) analysis of the role of atmospheric refractivity upon the electric field profiles; (4) comparison with the Very Low Frequency (VLF) electric field profiles measured by the Venera landers.

[7] *Simpson and Taflove* [2007] review Maxwell's equations modeling of impulsive subionospheric propagation in the ELF-VLF ranges using the finite difference time domain method, to assess heterogeneous and anisotropic media effects in wave propagation. In this work, we use a finite element algorithm similar to that developed for the cavity of Titan [*Simões et al.*, 2007] and other planetary environments [*Simões et al.*, 2008] where resonances can develop. We first recapitulate the theory of Schumann, and describe the numerical method for solving the surface-ionosphere cavity problem. We extend the 3D model to take into account corrections due to a non-negligible atmospheric density. After discussing the major input parameters proper to Venus, we estimate, both theoretical and numerically, the effect of atmospheric refractivity upon ELF wave propagation and compute the eigenfrequencies, Q-factors, and electric and magnetic field profiles of the cavity. Then, we evaluate the expected line splitting introduced by the day-night asymmetry of the cavity. We finally review the implications of the numerical results for wave propagation, validate the simulation technique against the data returned by the Venera landers, in the VLF range, and briefly present possible instruments and operation strategies for probing the electromagnetic environment of the Venus surface-ionosphere cavity.

2. Electromagnetic Wave Propagation in a Spherical Cavity

[8] An ionospheric cavity can be approximated by two conductive concentric spherical shells. A resonance develops whenever the average perimeter of the thin cavity is, to a first approximation, equal to an integral multiple of the wavelength. Hence, the angular resonant frequency is written

$$\omega_m = m\frac{c}{R}, \tag{1}$$

where R is the radius of the cavity, m = 1, 2,... is the eigenmode order and c is the velocity of light in the medium. Including a 3D spherical correction gives [*Schumann*, 1952]

$$\omega_m = \sqrt{m(m+1)}\,\frac{c}{R}. \tag{2}$$

[9] In addition to the Schumann or longitudinal resonance modes that, in the case of Venus, lie mostly in the ELF range, there are also, at higher frequencies, local transverse modes along the radial direction. In general, the formalism applicable to ELF wave propagation on Earth is also valid for Venus because the major characteristics of the two cavities are similar.

[10] The development of a general model for calculating Schumann resonances in the cavity of Venus requires the solution of Maxwell's equations, which are written

$$\nabla \times \boldsymbol{E} = -\frac{\partial \boldsymbol{B}}{\partial t}, \tag{3}$$

$$\nabla \times \boldsymbol{H} = \sigma \boldsymbol{E} + \frac{\partial \boldsymbol{D}}{\partial t}, \tag{4}$$

with

$$\boldsymbol{D} = \varepsilon\varepsilon_o \boldsymbol{E},\ \boldsymbol{B} = \mu_o \boldsymbol{H}, \tag{5}$$

where $\boldsymbol{E}$ and $\boldsymbol{D}$ are the electric and displacement fields, $\boldsymbol{H}$ and $\boldsymbol{B}$ are the magnetic field strength and flux density, ε_o and μ_o are the permittivity and magnetic permeability of vacuum, and ε and σ are the relative permittivity and conductivity of the medium, respectively.

[11] The system of equations (3)–(5) can be solved analytically in spherical coordinates for simple cavities, by considering the harmonic propagation approximation and decoupling the electric and magnetic fields [e.g., *Nickolaenko and Hayakawa*, 2002]. Assuming spherical symmetry for the cavity geometry and medium properties, namely neglecting the day-night asymmetry of the ionosphere, and the time dependence of the electromagnetic field, equations (3)–(4) can be decoupled in the standard method of separation of variables, which yields [*Bliokh et al.*, 1980]

$$\left\{\frac{d^2}{dr^2} - \frac{m(m+1)}{r^2} + \frac{\omega^2}{c^2}\varepsilon(r) - \sqrt{\varepsilon(r)}\,\frac{d^2}{dr^2}\left(\frac{1}{\sqrt{\varepsilon(r)}}\right)\right\}(r\phi(r)) = 0, \tag{6}$$

where r is the radial distance, ω is the angular frequency of the propagating wave and $\phi(r)$ is a function related to the electric and magnetic fields by the Debye potentials [*Wait*, 1962]. Equation (6) gives directly the eigenvalues of the longitudinal and transverse modes, which satisfy either

Table 1. Refractivities Measured and/or Evaluated for Radio Waves at 0°C and 1 atm[a]

Gas	ELF Refractivity
N_2	294
O_2	266
CO_2	494
H_2O vapor	61[b]
SO_2	686[c]
Earth dry air 78% N_2 + 21% O_2	288
Venus atmosphere (96.5% CO_2 + 3.5% N_2)	487

[a]After *Simões* [2007].
[b]20°C, 1.333 kPa.
[c]589.3 nm.

condition, $d\phi(r)/dr = 0$ or $\phi(r) = 0$, at both boundaries, respectively. In the limit of a thin void cavity, the eigenvalues of the longitudinal modes converge toward those calculated with equation (2).

[12] We shall now define three characteristic parameters of the cavity, namely the cavity quality factor, the atmospheric refractivity and skin depth in a medium:

[13] 1. The quality factor, or Q-factor, measures the wave attenuation in the cavity and is defined by

$$Q_m \equiv \frac{\mathrm{Re}(\omega_m)}{2\mathrm{Im}(\omega_m)} \approx \frac{\omega_m^{peak}}{\Delta\omega_m}, \tag{7}$$

where *Re* and *Im* are the real and imaginary parts of the complex eigenfrequency, ω_m^{peak} is the peak power frequency of mode *m,* and $\Delta\omega_m$ is the line width at half-power. The Q-factor measures the ratio of the accumulated field power to the power lost during one oscillation period.

[14] 2. The skin depth [*Balanis*, 1989],

$$\delta = \sqrt{\frac{2}{\mu_o \varepsilon_o}} \frac{1}{\omega\left(\sqrt{1+\left(\frac{\sigma}{\omega\varepsilon_o}\right)^2}-1\right)^{1/2}} \approx \sqrt{\frac{2}{\mu_o \sigma \omega}} \tag{8}$$

measures the distance over which the amplitude of the field is reduced by $e = 2.718$.

[15] 3. Finally, the refractivity, N, is related to the index of refraction, n, according to the definition

$$N \equiv (n-1) \times 10^6 \tag{9}$$

and is, to a first approximation, proportional to the gas density. We present the general approach of *Ciddor* [1996] to calculate air refractivity and subsequently apply the theory to Venus atmosphere.

[16] An atmosphere is a weakly dispersive medium, in particular for large wavelengths. The dispersion in a neutral gas is a function of composition and density, i.e., molecular structure, temperature, and pressure [e.g., *Bean and Dutton*, 1968]. We deal first with Earth and then turn toward Venus. Air refractivity is a function of pressure, temperature, and water vapor and is written

$$N_{air} = \frac{273.15}{101325}\frac{N_{g,ph}}{T}p - \frac{11.27 p_w}{T}, \tag{10}$$

where T [K] is the temperature, and p and p_w [Pa] are the air and partial water vapor pressures. The dispersive term, $N_{g,ph}$, where the indices g and ph refer to group and phase velocities, is given by the empirical relation:

$$N_{g,ph} = K + \frac{K_1}{\lambda^2} + \frac{K_2}{\lambda^4}, \tag{11}$$

where $K = 287.6155$ is the large wavelength limit, $K_1 = 4.88600$ or 1.62887 and $K_2 = 0.06800$ or 0.01360, for group and phase refractivity, respectively, and λ is the wavelength in μm [e.g., *Ciddor*, 1996; *Ciddor and Hill*, 1999]. These values are valid for standard dry air, i.e., 0°C, 101325 Pa, and 0.0375% of CO_2.

[17] The following simplifications are possible for ELF waves in the cavity of Venus: (1) the medium can be considered nondispersive because $K_j/\lambda \rightarrow 0$ in the ELF range, where $j = 1, 2$; (2) the weighted mean composition is assumed in the evaluation of the medium refractivity; (3) the refractivity is proportional to gas density: equation (10); (4) the water partial pressure and any correction due to the presence of SO_2 clouds are neglected. Table 1 shows the refractivities of selected gases at radio frequencies and Table 2 the refractivity of the atmosphere of Venus at various altitudes.

3. Numerical Model

3.1. Model Description

[18] Earlier cavity models were based upon a simplified parameterization, assumed spherical symmetry and did not take into account subsurface losses, soil properties, and atmospheric refractivity [*Nickolaenko and Rabinovich*, 1982; *Pechony and Price*, 2004; *Yang et al.*, 2006]. In this work, we solve equations (3)–(5) and evaluate the resonance modes with a finite element method [*Simões*, 2007; *Zimmerman*, 2006]. A preliminary version of this new model has already been applied to several planets, including Venus; this first approach included the properties of the subsurface material, but not the effects of cavity asymmetry and atmospheric refractivity [*Simões et al.*, 2008]. Surface losses can be neglected on Earth, but not on planets like Venus. The continuity conditions must therefore be imposed on the surface whenever the latter does not constitute the inner boundary of the cavity.

[19] The model sketched in Figure 1 includes the following parameters:

[20] 1. Permittivity profile of the atmosphere (ε_{atm}): In general, the permittivity of vacuum is assumed for the atmosphere but this is a crude approximation for Venus, because the pressure is high. Thus, a permittivity function that includes refractivity variation with altitude is introduced.

Table 2. Refractivity of the Atmosphere of Venus at Various Altitudes for 736 K and 92 atm on the Surface[a]

Altitude (km)	Environment	ELF Refractivity
0	736 K, 92 bar	16,600
32 (critical refraction)	465 K, 7 bar	2070
49.5	340 K, 1 bar	370

[a]Corresponding to a density of about 65 kg m^{-3}.

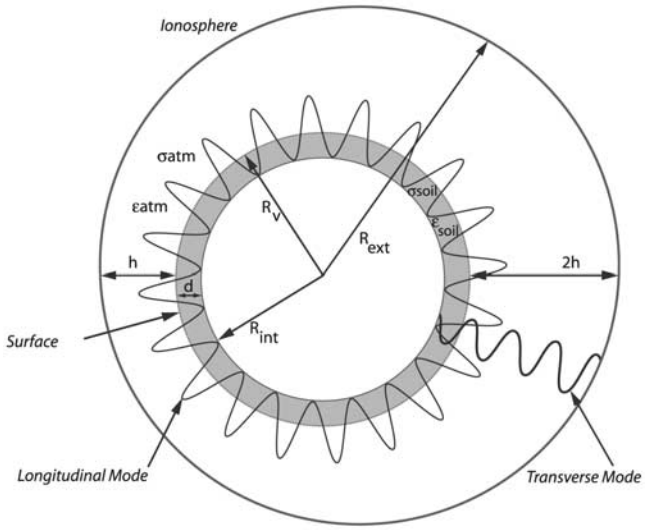

Figure 1. Sketch of the cavity model of Venus.

[21] 2. Conductivity profile of the atmosphere and lower ionosphere (σ_{atm}): The electron density has only been measured above ~120 km but the conductivity at lower altitude plays an important role in cavity losses. The conductivity profile includes Pioneer Venus and Magellan radio occultation data for altitudes higher than 120 km and a theoretical model below 80 km. Values in the range 80–130 km are obtained by interpolation.

[22] 3. Subsurface permittivity (e_{soil}). Pioneer Venus radar imaging yields an average surface permittivity of 5.0 ± 0.9 for the rolling plains and lowlands, and suggests that the surface is overlaid by at most only a few cm of soil or dust [*Pettengill et al.*, 1988]. *Campbell* [1994] has inferred a permittivity of ~4.15 using Magellan data. We use a constant permittivity value with depth in the range 4–10 to cover different soil compositions.

[23] 4. Subsurface conductivity (σ_{soil}): The composition of the surface includes many oxides, mainly silicon oxide, and the high temperature of the surface suggests that liquid phase materials are absent. Therefore, we consider surface conductivities in the range 10^{-6}–10^{-4} Sm^{-1} that match many oxide mixtures at ~750 K. The temperature variation with depth is also considered, which leads to specific conductivity profiles.

[24] 5. Height of the ionosphere (h) and cavity upper boundary (R_{ext}): The upper boundary of the cavity is located where the skin depth of propagating waves is much smaller than the separation between the shells. Therefore, the upper boundary is placed at $h \sim 130$ km at the subsolar point, where the skin depth is ~1 km for ELF waves. However, the slow rotation of the planet, specific atmospheric dynamics and chemistry, and the absence of a significant intrinsic magnetic field entail a highly asymmetric conductivity distribution. In a first attempt and for lack of data, we tentatively adjust the conductivity profile to a height of $2h$ at the subsolar point antipode, which requires a conductivity variation not only with the altitude but also with the separation from the subsolar point. This conductivity profile is somewhat arbitrary but, at least, provides a hint about the role of asymmetry on wave propagation. The effect is minor for Earth and corresponds to a small modification of the eigenmodes, but is more marked on Venus and may lead to eigenfrequency splitting.

[25] 6. Depth of the subsurface interface (d) and cavity lower boundary (R_{int}): The conductivity of the surface of Venus is expected to lie in the range 10^{-6}–10^{-4} Sm^{-1}, which implies a skin depth at shallow depths larger than 10 km. Therefore, the surface is not suitable as a PEC boundary and the inner shell must be placed lower down where the skin depth is less than, say, 1 km. In general, we shall assume $d = 100$ km in the current model that observes the previous condition.

[26] The model is solved not only in a 2D axisymmetric configuration, but also in 3D. The meshes are composed of ~10^4 and ~10^6 elements in 2D and 3D, respectively. Comparing the results obtained in 2D and 3D, whenever axial symmetry applies, assesses the algorithm accuracy. The numerical model includes two dedicated algorithms.

[27] 1. The eigenfrequency algorithm gives the complex frequencies of the eigenmodes, from which the Q-factors are derived. This solver uses the ARPACK numerical package based on a variant of the Arnoldi algorithm that is usually called the implicitly restarted Arnoldi method.

[28] 2. The harmonic propagation algorithm solves stationary problems with the UMFPACK numerical package, which computes frequency spectra, identifies propagating eigenmodes, calculates electric and magnetic fields over a wide altitude range and evaluates the influence of source distribution on the propagation modes. The harmonic propagation solver employs the unsymmetrical-pattern multifrontal method and direct LU-factorization (operator written as a product of a lower and upper triangular matrices) of the sparse matrix obtained by discretizing equations (3)–(5).

[29] The numerical algorithms have already been used and validated against the set of parameters applicable to the Earth cavity [*Simões et al.*, 2007, 2008]. The solvers and the finite element and unsymmetrical-pattern multifrontal methods are described by *Simões* [2007] and, in detail, by *Zimmerman* [2006].

3.2. Parameters Description

[30] Our knowledge of Venus has been gathered from ground-based observations and orbiter, flyby, balloon, and lander space missions. The properties of the upper ionosphere are measured with propagation techniques during radio occultation, but the electron density in the lower ionosphere and atmosphere is not known. Atmospheric data have been provided by several missions, including Voyager, Pioneer Venus, and Magellan, but the conductivity of the lower atmosphere is inferred from theoretical models.

[31] The atmospheric density profile is derived using pressure and temperature data obtained above ~34 km with propagation techniques, and surface in situ measurements performed by the Venera landers; the profile is then interpolated to match the gap at low altitude [e.g., *Hinson and Jenkins*, 1995; *Jenkins*, 1995]. Considering a carbon dioxide mole fraction of ~0.965, pressure and temperature of ~92 bar and ~736 K on the surface, the estimated atmospheric density is ~65 kgm^{-3}, which is about 55 times that on Earth. The relative permittivity, shown in Figure 2, is then obtained by using equations (9)–(11) and the refrac-

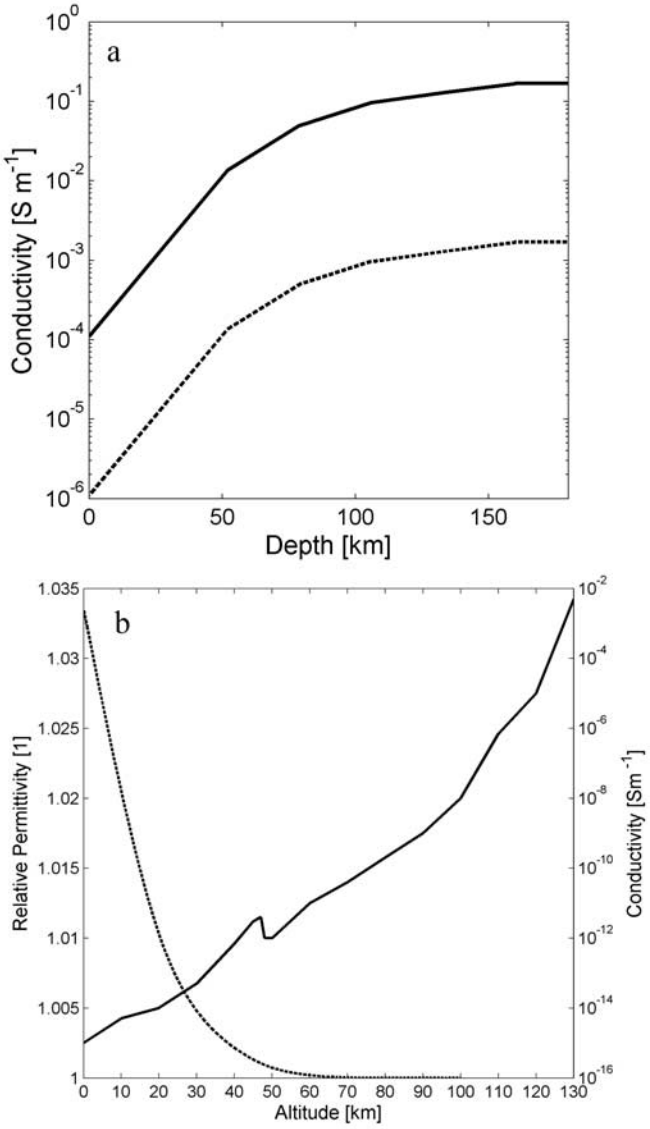

Figure 2. Permittivity and conductivity profiles in Venus's cavity. (a) Subsurface conductivity as a function of depth for high (solid curve) and low (dashed curve) soil conductivities; (b) conductivity (solid curve) and relative permittivity (dashed curve) of the atmosphere.

tivity reference values presented in Table 1. Though refractivity varies with wavelength in the visible and infrared it can be considered constant at lower frequencies. The relative permittivity, the square of the refractive index, is ~1.034 on the surface of Venus.

[32] The electron density and, consequently, the conductivity were measured with propagation techniques above ~120 km [e.g., *Brace et al.*, 1997]. Therefore, the profiles are only available for the upper part of the cavity, and a theoretical model is used to estimate the conductivity from 80 km down to the surface [*Borucki et al.*, 1982]. The conductivity is interpolated in the gap 80–120 km, between the measured and computed values at high and low altitudes, respectively.

[33] Volcanic processes, and many constructs and plains covered with extensive lava flows, dominate the surface of Venus. The radar altimeter onboard Pioneer Venus has shown that the radar-bright spots could be explained either by a roughness with a scale commensurate with the wavelength of the mapping signal, or by a larger dielectric constant of the surface material due to the presence of moderately conductive minerals such as iron sulphides and oxides. As written above, we use a relative permittivity in the range 4–10, whose values fit Venus analog materials. There is no evidence of significant water vapor concentration in the atmosphere or on the surface. Therefore, the soil might possess the conductivity of a desiccated igneous medium, such as basalt, at ~750 K. The surface conductivity is supposed to vary between 10^{-6} and 10^{-4} Sm^{-1}, supported by values measured on Earth for similar composition and temperature range [*Shanov et al.*, 2000; *Lide et al.*, 2005]. The conductivity profile (Figure 2) is a function of the interior temperature [*Arkani-Hamed*, 1994] in the depth range 0–180 km. The dielectric parameters are not dramatically different if high silica content is considered, and soil permittivity does not play a significant role because the soil conductivity is high enough.

[34] To simulate the day-night asymmetry, we consider in the first instance the transformation of conductivity $\sigma(r) \rightarrow \sigma(R_V + (r - R_V)(1 - 0.5 \times |\sin(\theta/2)|))$; that is, the conductivity profile is stretched so that the scale height at the subsolar point antipode is twice that at the subsolar point. The angle θ is measured with respect to the subsolar direction and axial symmetry is nevertheless preserved; R_V is the radius of Venus.

4. Wave Propagation in the Atmosphere

4.1. Ray Tracing Approximations

[35] The propagation of a wave in a cavity can be studied with the ray tracing technique, as long as the wavelength is less than the smallest dimension of the cavity and the relative variation of the refractive index is small over a commensurate distance. When either condition is not fulfilled, this approximation is no longer valid and a full wave approach is prerequisite.

[36] The permittivity of Earth's atmosphere is close to that of vacuum and, to a first approximation, does not play any significant role in the ELF range. However, the atmospheric conductivity profile and the associated wave attenuation must be taken into account when extreme accuracy is required in the determination of the Schumann frequencies. The situation is quite different on Venus, because of high atmospheric densities and pressure gradients.

[37] On Earth, tropospheric heterogeneities affect the propagation of waves within the broadcasting frequency ranges, which are sometimes detected outside their intended service area and interfere with other transmitter stations. In particular, the detection of radio waves much beyond the geometric horizon is evidence of inhomogeneous atmospheric conditions. This phenomenon is related to tropospheric ducting rather than reflection by the ionosphere. A duct acts as a waveguide; it consists of a layer with a relatively larger refractive index, and often develops during periods of stable weather. In a standard environment the density and the refractive index decrease with altitude in the troposphere. When a temperature inversion occurs, i.e., the temperature increases locally with height, a layer with a

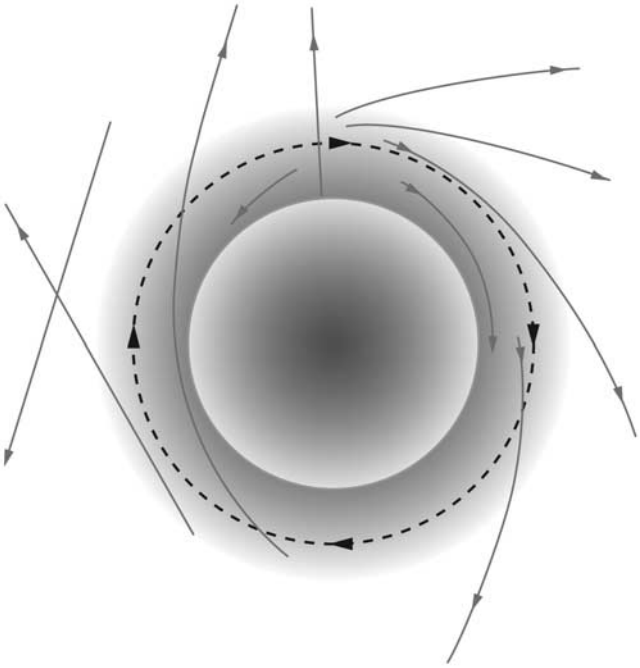

Figure 3. Schematic representation of atmospheric refraction. The dashed line represents the locus where refraction is balanced by curvature, which allows a wave to circle the planet.

higher refractive index might result. Radio waves are then partially trapped in the duct and can propagate beyond the horizon (Figure 3).

[38] At low frequencies, ray tracing provides a crude representation of wave paths in the cavity, and a qualitative understanding of refractivity phenomena. Using simple geometrical optics in spherical symmetry, one defines the refractive invariant along the raypath

$$n\,r\sin(z) = k, \tag{12}$$

where r is the radial distance, z the zenith angle, and k a constant. A simple, though accurate, geometric derivation of the well known refractive invariant, which can also be derived from Fermat's principle, is presented by A. T. Young (The refractive invariant, 2002, available at http://mintaka.sdsu.edu/GF/explain/atmos_refr/invariant.html, last accessed in October 2007). Differentiating equation (12) for z = 90° (horizontal elevation) yields

$$\frac{dn}{dr} = -\frac{n}{r} \Rightarrow \frac{dn}{dr} \approx -\frac{1}{r}. \tag{13}$$

[39] Maximum deviations of ~0.5° on Earth, and ~1° on Titan, can be computed from equations (12)–(13) with a ray tracing algorithm, for light rays with horizontal elevation. The situation is drastically different on Venus because of the strong atmospheric refractivity. In fact, it is possible to find an altitude where light rays with z = 90° circle the planet, provided that the attenuation is negligible.

[40] Figure 4 shows the refractivity gradient in the atmosphere of Venus as a function of altitude, derived from the permittivity profile presented in Figure 2. It is possible to derive from equation (13) the altitude at which a ray with horizontal elevation circles the planet. From $|\mathrm{dn}(\rho)/\mathrm{d}\rho| = 1/(R_v + \rho)$, where $\rho = r - R_V$, we obtain $\rho \approx 31.9$ km, corresponding to the horizontal dashed line, in close agreement with the altitude (33 km) derived by *Steffes et al.* [1994]. Rays with horizontal elevation below this threshold altitude are trapped in the atmosphere. The vertical dashed line at 34 km indicates the lowest altitude at which orbiter data are available. Rays departing from the surface with zenith angles larger than ~80° are trapped within the atmosphere. These phenomena seem to be associated with specific features of the ELF electric field profile.

4.2. ELF Wave Propagation Approximation

[41] The effects of atmospheric refractivity in wave propagation conditions on the ELF range can be assessed by solving equations (3)–(5) in spherical coordinates. Though aiming at different purpose, we use a similar approach to that developed by *Greifinger and Greifinger* [1978] and *Sentman* [1990] to calculate approximate Schumann resonance parameters for a two-scale-height conductivity profile of the Earth ionosphere. Unlike these models that use exponential conductivity profiles of the cavity, we neglect conductivity and consider an exponential permittivity profile instead. The relative permittivity profile of the atmosphere of Venus is rather similar to an exponential one (Figure 2). Making the usual separation of variables and considering the Lorentz gauge, the electric and magnetic fields of equations (3)–(5) can be transformed into the scalar, ψ, and vector, $\boldsymbol{A}$, potentials. Since the vector potential has

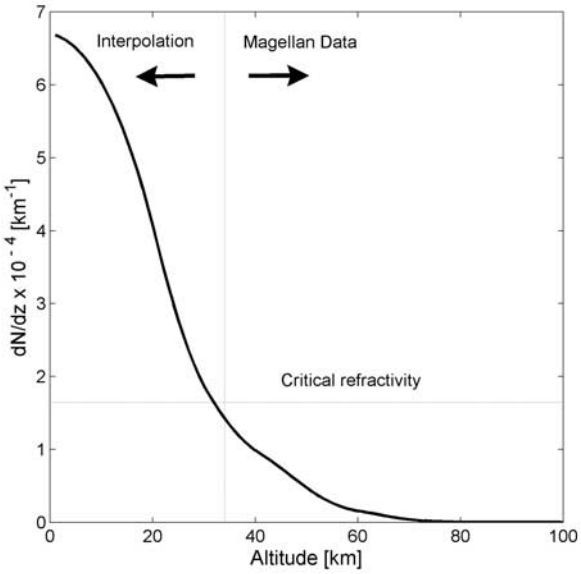

Figure 4. Refractivity gradient in the atmosphere of Venus as a function of altitude; the vertical dashed line marks the separation between the altitudes at which data have been collected from an orbiter ($h > 34$ km) and those at which the information results from an interpolation ($h < 34$ km); the horizontal dashed line identifies the refractivity gradient that balances curvature (curve intersection at 31.9 km).

Table 3. Eigenfrequencies for Several Lossless Cavity Configurations[a]

Configuration	First Eigenfrequency (Hz)	Second Eigenfrequency (Hz)	Third Eigenfrequency (Hz)
A	11.15	19.31	27.31
B	11.03	19.11	27.02
C	11.01	19.07	26.97
D	10.89	18.95	26.82
	(2×) 11.07	(2×) 18.99	(2×) 26.85
		(2×) 19.07	(2×) 26.88
			(2×) 26.92

[a]With $R_{int} = R_v$ and $R_{ext} = R_v + h$, where $h = 130$ km, and PEC boundary conditions: (A) using equation (2); (B) void cavity; (C) atmospheric permittivity profile given by Figure 2; and (D) asymmetric cavity with the atmospheric permittivity profile of C.

only a radial component, $\boldsymbol{A} = A_r$, the relation between the scalar and vector potentials can be written

$$\frac{\partial}{\partial r}\psi - i\omega\left(1 - m(m+1)\frac{c^2}{\omega^2 r^2 \varepsilon(r)}\right)A_r(r) = 0. \qquad (14)$$

[42] We shall assume an exponential atmospheric permittivity profile of the form

$$\varepsilon(r) = 1 + \varepsilon_s e^{-(r-R_v)/h_a} \qquad (15)$$

in the range $R_V \le r \le R_V + h$, $\varepsilon_s = 0.034$ corresponds to a permittivity correction close to the surface, and $h_a \approx 15.8$ km is the atmospheric permittivity scale height that best fits the data (Figure 2). Considering, to a first approximation, that the vector potential variation is negligible and differentiating equation (14), we find that the electric field has a maximum at the altitude

$$h_E = h_a \ln\left(\frac{R_V \varepsilon_s}{2h_a}\right). \qquad (16)$$

That is 29.6 km, an altitude similar to that calculated with the ray tracing approximation. The maximum of equation (14) is independent of frequency as long as the vector potential can be considered constant; hence, the same maximum is obtained in the ELF and VLF ranges. The correction due to the permittivity profile deviation from an exponential law is calculated numerically.

5. Results and Discussion

5.1. Modeling Results

[43] In this section we compare the results obtained with analytical approximations, full wave propagation numerical models, and ray tracing techniques; we also assess the effects of surface losses and asymmetric cavity configuration upon wave propagation.

[44] Tables 3 and 4 show the eigenfrequencies for several cavity configurations with lossless and lossy media, respectively. The corrections associated with the atmospheric permittivity profile are small compared with those due to the cavity losses associated with the conductivity profile. Cavity asymmetry partially removes eigenmode degeneracy, in particular for the lowest eigenfrequency, where splitting can be higher than 1 Hz for a lossy medium. The degeneracy of the eigenmodes is not completely removed because axial symmetry remains; hence partially degenerated lines exist for each eigenfrequency. In fact, each eigenstate m is $(2m + 1)$-fold degenerate for a symmetric cavity, but day-night asymmetry partially removes degeneracy and produces $m + 1$ lines, which means that all lines but one are doubly degenerate.

[45] On Earth, the upper boundary of the cavity does not have a spherical shape because several processes contribute to ionospheric layer distortion and, therefore, eigenfrequency degeneracy is removed. The most significant contributions are due to day-night asymmetry, polar heterogeneity, and intrinsic geomagnetic field. According to numerical calculations made by *Galejs* [1972], frequency splitting due to day-night asymmetry is small. Consequently, the corrections introduced by the polar heterogeneity and geomagnetic field are dominant. On the contrary, the major contribution to line splitting on Venus comes from day-night asymmetry because the ionosphere is highly deformed and other contributions can be neglected in a first-order approximation. Recent observations have shown evidence of line splitting (∼0.5 Hz) and amplitude variation of Schumann resonances of the Earth's cavity due to cavity asymmetry

Table 4. Eigenfrequencies for Several Cavity Configurations as Functions of Subsurface Properties and Medium Losses[a]

Configuration	First Eigenfrequency (Hz)	Second Eigenfrequency (Hz)	Third Eigenfrequency (Hz)
A	$9.13 + 0.62i$	$16.22 + 1.01i$	$23.22 + 1.32i$
B	$8.85 + 0.75i$	$15.79 + 1.21i$	$22.70 + 1.62i$
C	$8.11 + 0.94i$	$14.61 + 1.51i$	$21.11 + 2.04i$
D	(2×) $9.28 + 0.34i$	(2×) $15.53 + 0.62i$	(2×) $21.48 + 0.95i$
	$10.61 + 0.19i$	$17.28 + 0.23i$	(2×) $24.71 + 0.64i$
		(2×) $17.93 + 0.52i$	(2×) $24.93 + 0.87i$
			$25.07 + 0.61i$

[a]With $R_{int} = R_v - d$ and $R_{ext} = R_v + h$, and $h = 130$ km. Atmospheric permittivity and conductivity profiles are those of Figure 2. (A) Symmetric cavity and d = 0 (PEC surface); (B) d = 100 km and high-conductivity subsurface profile; (C) same as B, but with low-conductivity subsurface profile; (D) asymmetric cavity with d = 0 and conductivity profile function of radius and angle (see text for details).

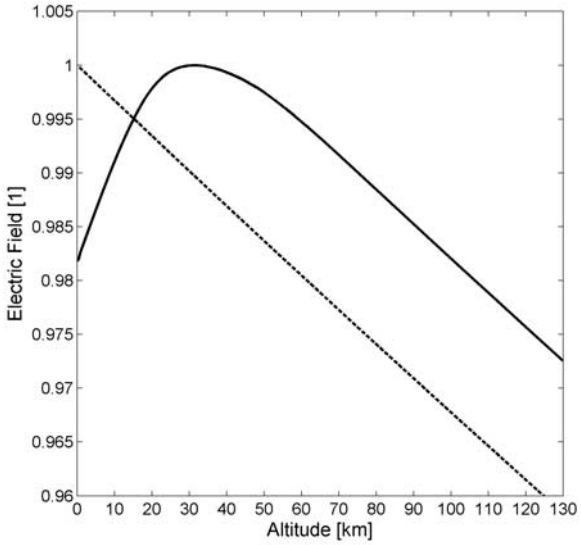

Figure 5. Electric field amplitude as a function of altitude in a lossless cavity with PEC boundaries, where $R_{int} = R_v$, $R_{ext} = R_v + h$, and $h = 130$ km. The permittivity is given by the profile of Figure 2 (solid curve) or is assumed to be that of vacuum (dashed curve). The electric field maximum is reached at an altitude of 31.5 km.

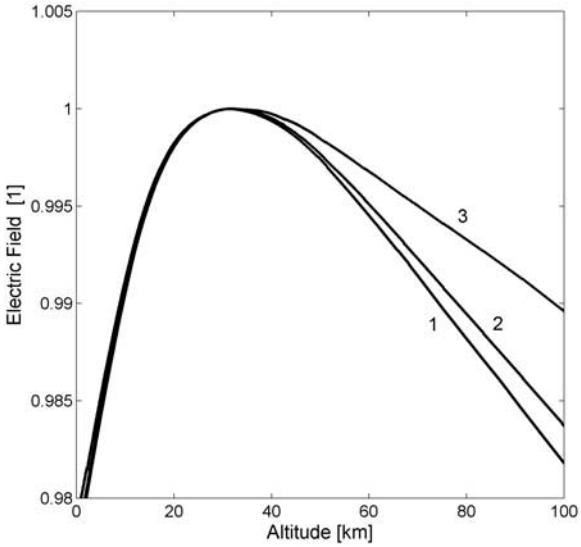

Figure 7. Electric field, in arbitrary units, as a function of altitude for various frequencies: (1) 1–100 Hz; (2) 1 kHz; (3) 10 kHz. The electric field maximum is located at approximately 31.5 km for all frequencies. The cavity configuration is the same as in Figure 5.

[*Sátori et al.*, 2007; *Nickolaenko and Sentman*, 2007]. According to the present model, eigenfrequency splitting for the Venus cavity is higher than for Earth because of not only larger cavity asymmetry but also higher Q-factor. Thus, the Venus cavity spectrum has distinctive peaks because the distance between adjacent split lines is larger and higher Q-factors produce better resolved peaks. Therefore, if Schumann resonances are excited in the cavity, frequency splitting due to day-night asymmetry should be unambiguously detected on Venus.

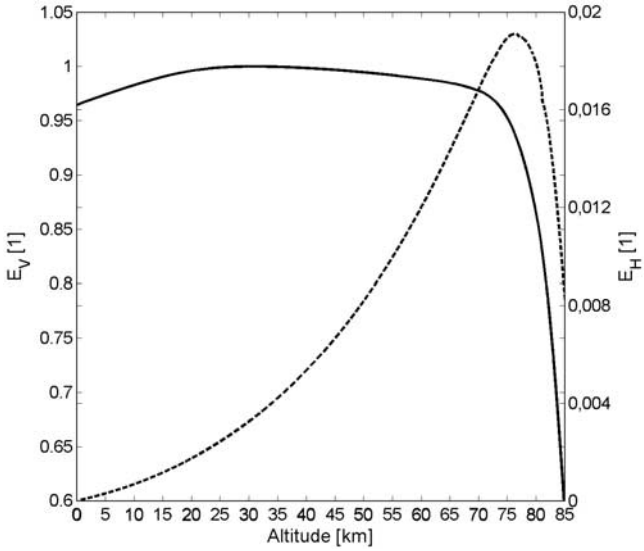

Figure 6. Vertical (E_V, solid curve) and horizontal (E_H, dashed curve) electric field components as functions of altitude up to 85 km in a cavity where $R_{int} = R_v$, $R_{ext} = R_v + h$, and $h = 130$ km, PEC boundary conditions, and permittivity and conductivity profiles of Figure 2. The values are normalized with respect to the electric field at 31.5 km.

[46] Although the ELF wave propagation and ray tracing models cannot be strictly compared, it is interesting to note that they predict similar altitudes for the maximum of the electric field (29.6 and 31.5 km for analytical and numerical approximations, respectively) and the ray that circles the planet at constant altitude (31.9 km). In fact, as shown in Figure 5, the presence of a heterogeneous atmosphere refracts waves, which are preferentially focused at a particular altitude. Furthermore, introducing temperature lapse rate inversion, i.e., increasing density with altitude, allows the formation of local electric field maxima in a straightforward manner. The higher difference obtained with the analytical model is due to the assumed exponential permittivity profile, which is only valid in a first approximation.

[47] As on Earth, the thickness of the cavity is small with respect to the radius and, therefore, the horizontally polarized electric field (E_H) is almost 2 orders of magnitude smaller than the vertically polarized electric field (E_V) (Figure 6). The corrections to the vertical and horizontal electric field components due to a lossy surface are small. A different scenario is expected on Titan where $E_H/E_V \sim 0.1$ because of the smaller cavity radius and larger surface-ionosphere distance [*Simões et al.*, 2007].

[48] Figure 7 shows the electric field amplitude at several frequencies in the range 1 Hz – 10 kHz. The electric field profiles are similar and show a peak roughly at the same altitude. The model was also run at higher frequencies but did not provide accurate results. In fact, higher frequencies require a finer mesh, which implies additional memory. This numerical limitation also indicates to what extent atmo-

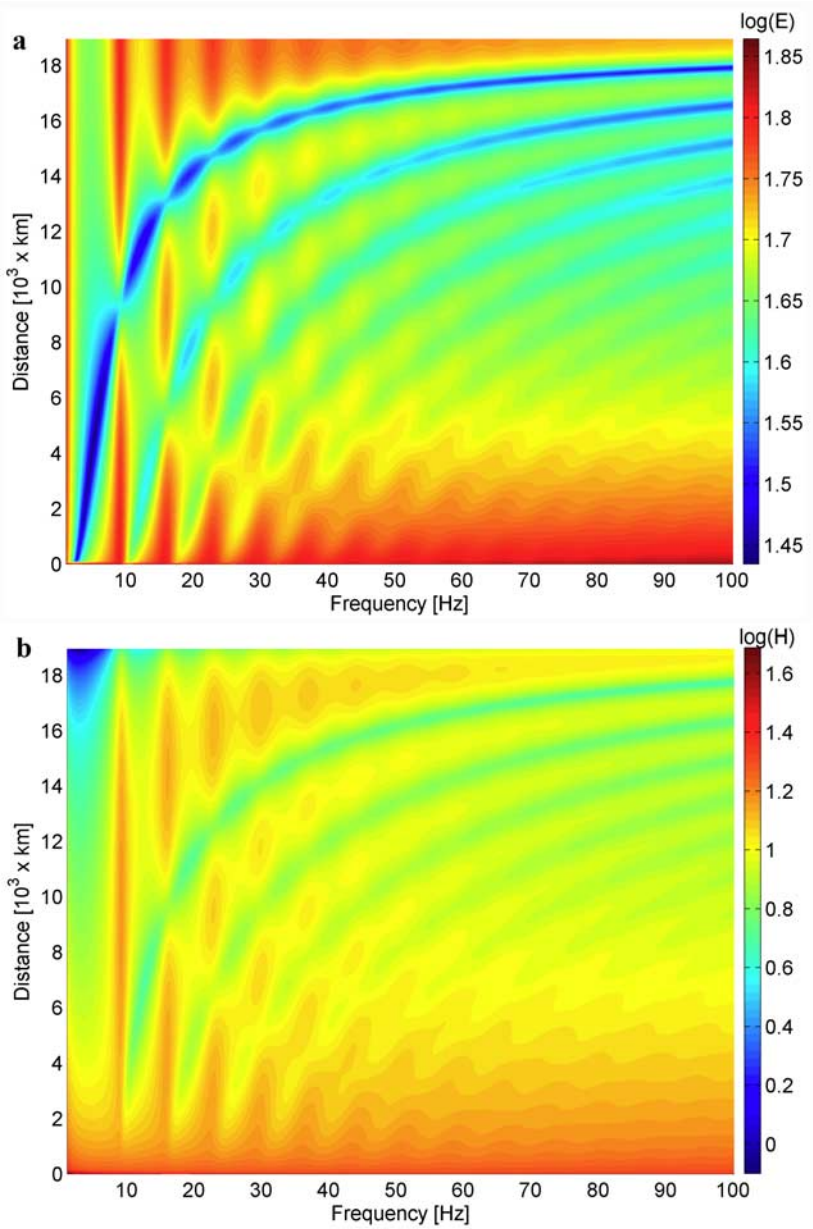

Figure 8. Maps of electric (a) and magnetic (b) fields in the ELF range as functions of frequency and source distance with the cavity configuration of Figure 6. Field amplitudes are in arbitrary units.

spheric heterogeneities distort the electric field profile and is useful to assess the effect of atmospheric turbulence.

[49] Figure 8 presents maps of the electric and magnetic fields amplitude distribution as functions of the source-receiver distance. The cavity parameterization is: $R_{int} = R_v$ and $R_{ext} = R_v + h$, where h = 130 km, PEC boundary conditions, and the permittivity and conductivity profiles of Figure 2. The electromagnetic source is a vertical Hertz dipole of 20 km length at an altitude of 50 km. The dipole is stationary, with uniform spectral radiance and arbitrary amplitude in the ELF range. On the maps shown in Figure 8, frequency is measured along the abscissa and distance between source and receiver along the ordinate; amplitude is given by a color logarithmic scale in arbitrary units, for better visualization. As the source-receiver distance increases, the spectral peak rapidly decays, and the resonance frequency is shifted with distance; the nodes of the electric field correspond to the antinodes of the magnetic field, and vice versa. Finally, the amplitude of the electric field increases when one approaches the source location or its antipode; no eigenmodes are observed in various sectors where the field amplitude is small. Comparison with similar maps computed for the cavity of Earth shows that the general features are similar but that the eigenmodes are more clearly identified on Venus. In fact, Venus spectra are sharper and less shifted because of lower losses in the cavity.

Table 5. Eigenfrequencies and Q-Factors for Several Models With a Perfectly Reflecting Surface[a]

	First Mode		Second Mode		Third Mode	
Model	Frequency (Hz)	Q	Frequency (Hz)	Q	Frequency (Hz)	Q
M1	9.0	5.1	15.8	5.1	22.7	5.2
M2	9.3	10.5	16.3	11.3	23.3	11.7
M3	9.05	10.07	15.9	10.23	22.64	10.31
M4	9.01	8.0	15.81	8.1	22.74	8.0
M5	9.13	7.5	16.22	8.0	23.22	8.8

[a]Model: M1, *Nickolaenko and Rabinovich* [1982]; M2, *Pechony and Price* [2004]; M3, *Yang et al.* [2006]; M4, *Simões et al.* [2008]; M5, Table 4, configuration A.

[50] The properties of the Venus regolith lie between those of the highly conductive soil of Earth and those of the almost dielectric-like surface of Titan. The surface of Earth can be considered as a PEC boundary, which means the subsurface contribution to the cavity is negligible and soil permittivity can be ignored. On the contrary, the surface conductivity of Titan is extremely low and the surface is no longer the inner boundary, because the skin depth for ELF waves is significant. There, the soil complex dielectric properties must be taken into account, which includes not only the conductivity, but also the permittivity, variations with depth. On Venus, the range of the expected subsurface dielectric properties is such that the soil conductivity must be taken into account, but not the permittivity. Table 4 shows the three lowest complex eigenfrequencies calculated with several cavity configurations and subsurface contribu-

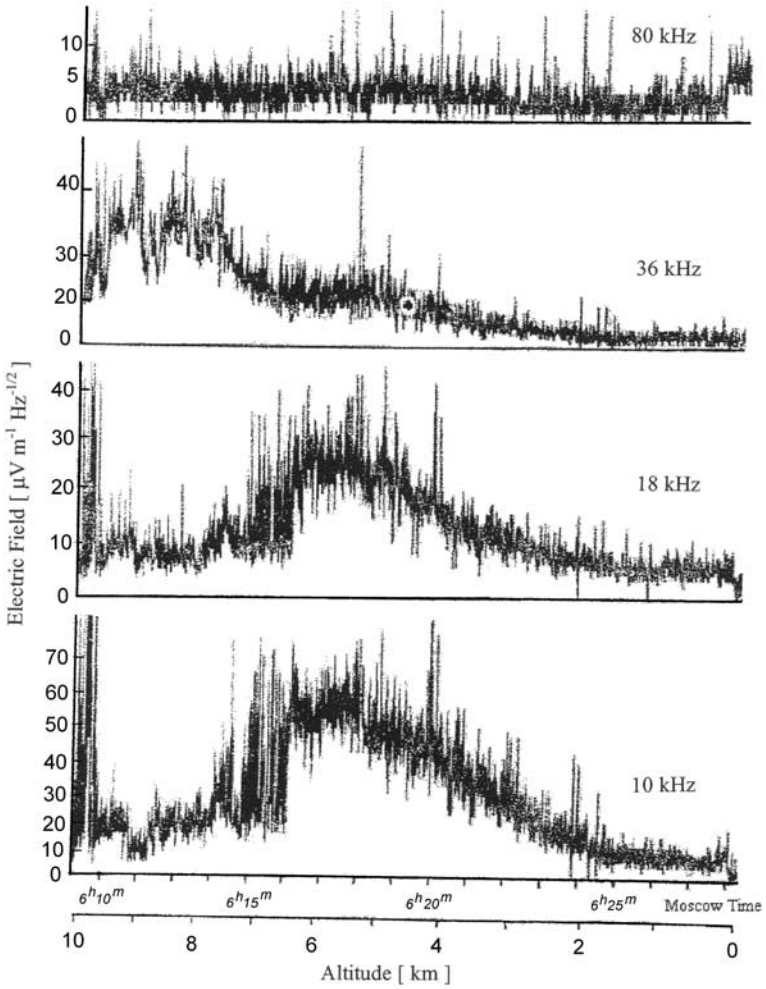

Figure 9. Electric field measurements performed by Venera 11 in the altitude range 0–10 km [after *Ksanfomaliti et al.*, 1979]. Modified from *Ksanfomaliti et al.* [1979] with kind permission of Springer Science and Business Media.

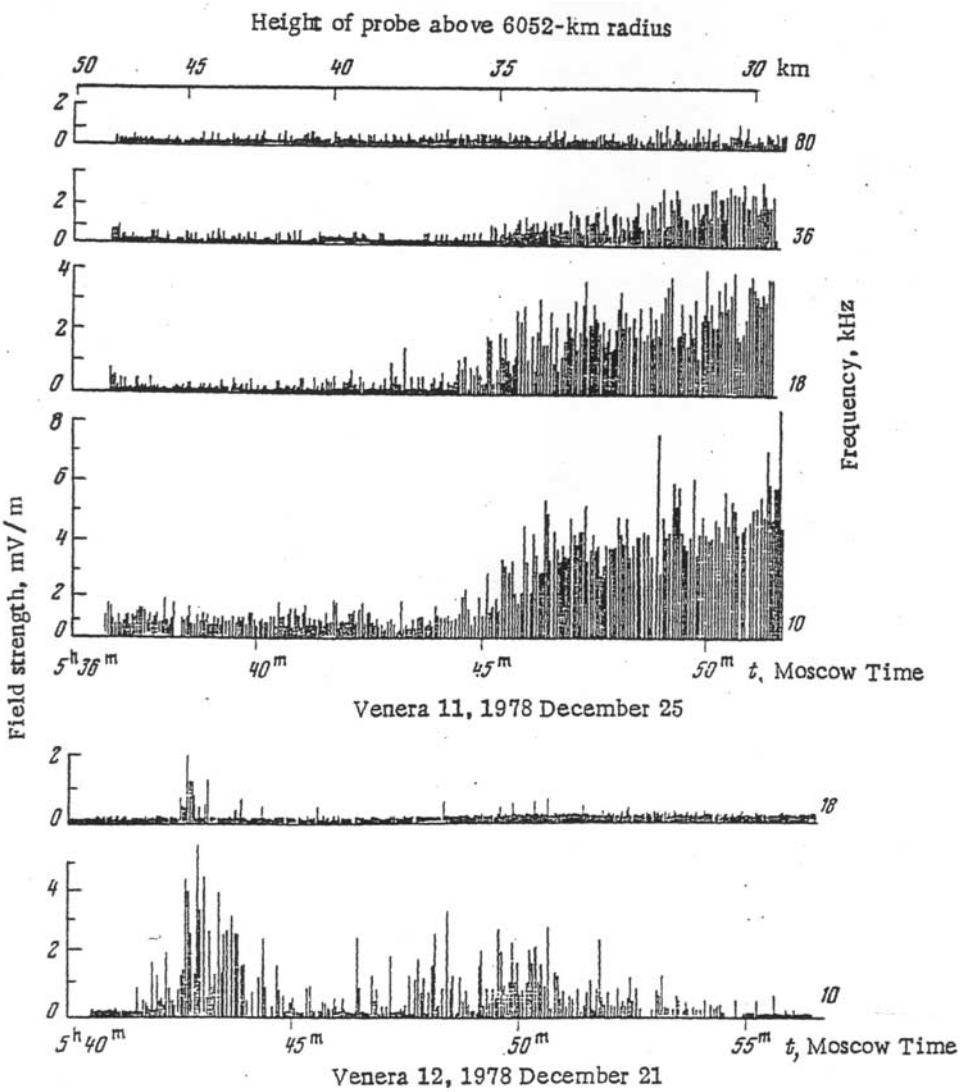

Figure 10. Electric field measurements performed by Venera 11 (top) and 12 (bottom) in the altitude range 30–50 km [after *Ksanfomaliti et al.*, 1979]. Modified from *Ksanfomaliti et al.* [1979] with kind permission of Springer Science and Business Media.

tions. The Q-factor can be calculated using equation (7), which yields values of the order of 8, 6.5, and 5 for configurations A, B, and C, respectively. These values are larger than for Earth, suggesting that ELF waves are less attenuated on Venus. It is interesting to compare the results obtained for the configurations B and C; in this case, lower soil conductivity implies higher losses but that is not universal because competing mechanisms can balance each other. The dielectric losses of the medium tend to decrease the Q-factor, whereas the lower inner radius increases the eigenfrequencies, as previously reported by *Simões et al.* [2007] for the cavity of Titan.

[51] Table 5 summarizes the results computed by *Nickolaenko and Rabinovich* [1982] (M1), *Pechony and Price* [2004] (M2), *Yang et al.* [2006] (M3), *Simões et al.* [2008] (M4), and the output from the current model (M5). Comparing these results leads to the following conclusions: (1) the models predict similar frequencies for the three lowest eigenmodes if the same conductivity profile and the PEC surface are considered (M1–M5); (2) the atmospheric permittivity profile introduces minimal corrections on eigenfrequencies (for comparison, see Tables 4 and 5); (3) subsurface losses decrease eigenfrequencies and Q-factors (for comparison, see Tables 4 and 5); (4) whereas the Q-factors of M1 are similar for the three lowest eigenmodes, those of M2 and M3 increase with frequency. According to *Yang et al.* [2006], the utilization of different equations to derive the Q-factors explain the discrepancies between M1 and M2–M3. On the contrary, M4 and M5 take in consideration the definition of the Q-factor, i.e., equation (7), and should be more reliable. Nevertheless, further studies are required to assess whether the Q-factors on Venus are functions of frequency, like on Earth.

5.2. Comparison With Observations and Future Measurements

[52] The Venera Landers 11 and 12 carried a low-frequency spectrum analyzer consisting of four channels

with central frequencies at 10, 18, 36, and 80 kHz and bandwidths of 1.6, 2.6, 4.6, and 14.6 kHz, respectively. The experimental results (see Figures 9 and 10) exhibit the following features: (1) for both landers the power decreases with increasing frequency; (2) the spectral power increases below 35 km for Venera 11, and between 50 and 30 km for Venera 12; (3) the noise decreases below 10 km on Venera 11 data; (4) the noise on both landers significantly decreases close to the surface; (5) the noise shows local maxima in the various channels of both landers in the altitude range 3–8 km [*Ksanfomaliti et al.*, 1979].

[53] Comparison between the present model predictions and the Venera landers data shows that the electric field profiles are moderately consistent. However, detailed analyses would require continuous electric field profiles below 50 km down to the surface; whereas the increase of electric field is observed below 35 km, it is not clear whether a maximum exists at about 30 km. Nevertheless, the electric field amplitude decreases close to the surface. The maxima at about 5 km in the Venera data could be due to a local temperature inversion.

[54] The vertical electric and horizontal magnetic fields can be measured on Venus, as on Earth, with vertical dipole and loop antennas. The design of the antennas is often imposed by the mission, as illustrated by the configurations proposed by *Berthelier et al.* [2000] for the surface of Mars and that used onboard the Huygens Probe in the atmosphere of Titan [*Grard et al.*, 1995; *Falkner*, 2004]. Waveform recording facilitates data analysis, but onboard spectral processing is generally more convenient because of computer memory constraints. However, the most important parameter is frequency resolution, which should be of the order of 0.1 Hz to measure the Q-factor of the resonances and resolve any line splitting of the eigenfrequencies.

[55] Because of vehicle vibrations induced by airflow, it is easier to measure Schumann resonances on a stationary platform rather than during ascent or descent. Electrostatic and ELF electromagnetic noise decrease instrument sensitivity and limit the measurement threshold to about a fraction of 1 mV for vertical antennas. Static modules on the surface or balloons floating at a constant atmospheric pressure minimize turbulence and antenna vibrations. For example, the number of Schumann resonances identified on a stratospheric balloon is lower than in a quiet environment, which confirms that the vehicle trajectory and dynamics impose significant constraints on the measurement.

6. Conclusions

[56] The distinctive properties of the Venus atmosphere strongly influence the propagation of ELF and VLF electromagnetic waves in the cavity. The atmospheric density does not significantly modify the eigenfrequencies because the relative permittivity does not exceed $\sim$1.034 close to the surface, but the density gradient produces a peak on the ELF electric field profile (Figure 5). Wave attenuation is probably less than on Earth (Table 4); the surface of Venus is not a PEC boundary, and subsurface losses contribute further to the intricacy of the cavity.

[57] The high refractivity of Venus atmosphere facilitates ducting phenomena and propagation beyond the geometric horizon. Under certain conditions, electromagnetic waves can travel at a constant altitude ($\sim$31.9 km) because planetary curvature can be balanced by atmospheric refraction (see sketch in Figure 3). This phenomenon preferentially focuses electromagnetic waves at midaltitudes: (1) according to our analytical approximation and considering an exponential atmospheric permittivity profile, the electric field maximum is located at an altitude of 29.6 km; (2) the numerical model that uses a more accurate profile predicts 31.5 km. The overall model is, to some extent, consistent with the experimental profile recorded by the Venera Probes (Figure 9), in particular with the electric field decrease below 10 km (Figure 10).

[58] The predicted eigenfrequencies are roughly 1 Hz higher on Venus than on Earth and the Q-factors are higher than 6, which implies lower attenuation. Further studies are required to assess whether the Q-factors vary with frequency. The three major reasons for Schumann resonance splitting at Earth are day-night asymmetry, polar nonuniformity and, most importantly, the existence of an intrinsic geomagnetic field. On Venus, on the contrary, the day-night asymmetry is clearly the dominant contribution and can remove eigenfrequency degeneracy and split the lines by more than 1 Hz, depending upon the shape of the cavity (Tables 3 and 4). Besides, the higher Q-factors of the Venus cavity provide better resolved peaks that make the detection of line-splitting easier than on Earth.

[59] The addition of electric and magnetic antennas, amplifiers and signal processing equipment to the payloads of buoyant probes (balloons, airships, and descent crafts) and landers, to measure the vertical and horizontal polarization profiles of ELF electromagnetic fields in the altitude range 0–100 km (Figure 6), provides a powerful tool for studying wave propagation and atmospheric dynamics in the Venus cavity. Such investigations would ascertain the presence of electromagnetic sources in the cavity, and confirm the existence of lightning activity on Venus.

[60] **Acknowledgments.** The authors thank the International Space Science Institute (Bern, Switzerland) for hosting and supporting their team meetings. The first author is indebted to Alain Péan (CETP, France) for fruitful discussions about software and hardware optimization and to Hugo Simões (ESA-ESTEC, Netherlands) for artwork. The authors thank the referees, namely Olga Pechony, for their valuable and pertinent comments that contributed to the improvement of this manuscript.

References

Arkani-Hamed, J. (1994), On the thermal evolution of Venus, *J. Geophys. Res.*, *99*, 2019–2033, doi:10.1029/93JE03172.

Balanis, C. A. (1989), *Advanced Engineering Electromagnetics*, 1008 pp., Wiley, New York.

Balser, M., and C. A. Wagner (1960), Observations of Earth-ionosphere cavity resonances, *Nature*, *188*, 638–641, doi:10.1038/188638a0.

Bean, B. R., and E. J. Dutton (1968), *Radio Meteorology*, 435 pp., Dover Publ., New York.

Béghin, C., et al. (2007), A Schumann-like resonance on Titan driven by Saturn's magnetosphere possibly revealed by the Huygens Probe, *Icarus*, *191*, 251–266, doi:10.1016/j.icarus.2007.04.005.

Berthelier, J. J., R. Grard, H. Laakso, and M. Parrot (2000), ARES, atmospheric relaxation and electric field sensor, the electric field experiment on NETLANDER, *Planet. Space Sci.*, *48*, 1193–1200.

Besser, B. P. (2007), Synopsis of the historical development of Schumann resonances, *Radio Sci.*, *42*, RS2S02, doi:10.1029/2006RS003495.

Bliokh, P. V., A. P. Nickolaenko, and Y. F. Filippov (1980), *Schumann Resonances in the Earth-Ionosphere Cavity*, edited by D. L1. Jones, 175 pp., Peter Peregrinus, Oxford, UK.

Borucki, W. J., Z. Levin, R. C. Whitten, R. G. Keesee, L. A. Capone, O. B. Toon, and J. Dubach (1982), Predicted electrical conductivity between

0 and 80 km in the Venusian atmosphere, *Icarus*, *51*, 302–321, doi:10.1016/0019-1035(82)90086-0.

Brace, L. H., J. M. Grebowsky, and A. J. Kliore (1997), Pioneer Venus orbiter contributions to a revised Venus reference ionosphere, *Adv. Space Res.*, *19*(8), doi:10.1016/S0273-1177(97)00271-8.

Campbell, B. A. (1994), Merging Magellan emissivity and SAR data for analysis of Venus surface dielectric properties, *Icarus*, *112*, 187–203, doi:10.1006/icar.1994.1177.

Ciddor, P. E. (1996), Refractive index of air: New equations for the visible and near infrared, *Appl. Opt.*, *35*, 1566–1573.

Ciddor, P. E., and R. J. Hill (1999), Refractive index of air: 2. Group index, *Appl. Opt.*, *38*, 1663–1667.

Falkner, P. (2004), Permittivity, waves and altimeter analyser for the ESA/NASA Cassini-Huygens Project (in German) Ph.D. thesis, Tech. Univ. of Graz, Austria.

Galejs, J. (1972), *Terrestrial Propagation of Long Electromagnetic Waves*, 362 pp., Pergamon, New York.

Grard, R., H. Svedhem, V. Brown, P. Falkner, and M. Hamelin (1995), An experimental investigation of atmospheric electricity and lightning activity to be performed during the descent of the Huygens Probe on Titan, *J. Atmos. Terr. Phys.*, *57*, 575–585, doi:10.1016/0021-9169(94)00082-Y.

Greifinger, C., and P. Greifinger (1978), Approximate method for determining ELF eigen-values in the Earth-ionosphere waveguide, *Radio Sci.*, *13*(5), 831–837.

Gurnett, D. A., W. S. Kurth, A. Roux, R. Gendrin, C. F. Kennel, and S. J. Bolton (1991), Lightning and plasma wave observations from the Galileo flyby of Venus, *Science*, *253*, 1522–1525, doi:10.1126/science.253.5027.1522.

Gurnett, D. A., P. Zarka, R. Manning, W. S. Kurth, G. B. Hospodarsky, T. F. Averkamp, M. L. Kaiser, and W. M. Farrell (2001), Non-detection at Venus of high-frequency radio signals characteristic of terrestrial lightning, *Nature*, *409*, 313–315, doi:10.1038/35053009.

Hansell, S. A., W. K. Wells, and D. M. Hunten (1995), Optical detection of lightning on Venus, *Icarus*, *117*, 345–351, doi:10.1006/icar.1995.1160.

Hinson, D. P., and J. M. Jenkins (1995), Magellan radio occultation measurements of atmospheric waves on Venus, *Icarus*, *114*, 310–327, doi:10.1006/icar.1995.1064.

Jenkins, J. M. (1995), Reduction and analysis of seasons 15 and 16 (1991–1992) Pioneer Venus radio occulation data and correlative studies with observations of the near infrared emission of Venus, technical report, 15 pp., NASA/ARC, Moffett Field, Calif.

Krasnopol'sky, V. A. (1980), Lightning on Venus according to information obtained by the satellites Venera 9 and 10, *Kosm. Issled.*, *18*, 429–434.

Ksanfomaliti, L. V. (1979), Lightning in the cloud layer of Venus, *Kosm. Issled.*, *17*, 747–762.

Ksanfomaliti, L. V., N. M. Vasil'chikov, O. F. Ganpantserova, E. V. Petrova, A. P. Suvorov, G. F. Filipov, O. V. Yablonskaya, and L. V. Yabrova (1979), Electrical discharges in the atmosphere of Venus, *Sov. Astron. Lett.*, *5*(3), 122–126.

Lide, D. R., et al. (2005), *CRC Handbook of Chemistry and Physics*, 86th ed., 2544 pp., Taylor and Francis, Boca Raton, Fla.

Nickolaenko, A. P., and M. Hayakawa (2002), *Resonances in the Earth-Ionosphere Cavity*, Kluwer Acad., 380 pp., Dordrecht, Netherlands.

Nickolaenko, A. P., and L. M. Rabinovich (1982), The possibility of existence of global electromagnetic resonances on solar-system planets, *Kosm. Issled.*, *20*, 82–88.

Nickolaenko, A. P., and D. D. Sentman (2007), Line splitting in the Schumann resonance oscillations, *Radio Sci.*, *42*, RS2S13, doi:10.1029/2006RS003473.

Pechony, O., and C. Price (2004), Schumann resonance parameters calculated with a partially uniform knee model on Earth, Venus, Mars, and Titan, *Radio Sci.*, *39*, RS5007, doi:10.1029/2004RS003056.

Pettengill, G. H., P. G. Ford, and B. D. Chapman (1988), Venus: Surface electromagnetic properties, *J. Geophys. Res.*, *93*, 14,881–14,892, doi:10.1029/JB093iB12p14881.

Price, C. (2000), Evidences for a link between global lightning activity and upper tropospheric water vapour, *Lett. Nature*, *406*, 290–293, doi:10.1038/35018543.

Price, C., O. Pechony, and E. Greenberg (2007), Schumann resonances in lightning research, *J. Lightning Res.*, *1*, 1–15.

Russell, C. T. (1991), Venus lightning, *Space Sci. Rev.*, *55*, 317–356.

Russell, C. T. (1993), Planetary lightning, *Annu. Rev. Earth Planet. Sci.*, *21*, 43–87, doi:10.1146/annurev.ea.21.050193.000355.

Russell, C. T., T. L. Zhang, M. Delva, W. Magnes, R. J. Strangeway, and H. Y. Wei (2007), Lightning on Venus inferred from whistler-mode waves in the ionosphere, *Nature*, *450*, 661–662, doi:10.1038/nature05930.

Sátori, G., M. Neska, E. Williams, and J. Szendroi (2007), Signatures of the day-night asymmetry of the Earth-ionosphere cavity in high time resolution Schumann resonance records, *Radio Sci.*, *42*, RS2S10, doi:10.1029/2006RS003483.

Schumann, W. O. (1952), On the free oscillations of a conducting sphere which is surrounded by an air layer and an ionosphere shell (in German), *Z. Naturforsch. A*, *7*, 149–154.

Sentman, D. D. (1990), Approximate Schumann resonance parameters for a two-scale height ionosphere, *J. Atmos. Terr. Phys.*, *52*, 35.

Shanov, S., Y. Yanev, and M. Lastovickova (2000), Temperature dependence of the electrical conductivity of granite and quartz-monzonite from south Bulgaria: Geodynamic inferences, *J. Balkan Geophys. Soc.*, *3*, 13–19.

Simões, F. (2007), Theoretical and experimental studies of electromagnetic resonances in the ionospheric cavities of planets and satellites; instrument and mission perspectives, Ph.D. thesis, 283 pp., Univ. Pierre et Marie Curie, Paris.

Simões, F., et al. (2007), A new numerical model for the simulation of ELF wave propagation and the computation of eigenmodes in the atmosphere of Titan: Did Huygens observe any Schumann resonance?, *Planet. Space Sci.*, *55*, 1978–1989, doi:10.1016/j.pss.2007.04.016.

Simões, F., R. Grard, M. Hamelin, J. J. López-Moreno, K. Schwingenschuh, C. Béghin, J.-J. Berthelier, J.-P. Lebreton, G. J. Molina-Cuberos, and T. Tokano (2008), The Schumann resonance: A tool for exploring the atmospheric environment and the subsurface of the planets and their satellites, *Icarus*, *194*, 30–41, doi:10.1016/j.icarus.2007.09.020.

Simpson, J. J., and A. Taflove (2007), A review of progress in FDTD Maxwell's equations modeling of impulsive subionospheric propagation below 300 kHz, *IEEE Trans. Antennas Propag.*, *55*, 1582–1590, doi:10.1109/TAP.2007.897138.

Steffes, P. G., J. M. Jenkins, R. S. Austin, S. W. Asmar, D. T. Lyons, E. H. Seale, and G. L. Tyler (1994), Radio occultation studies of the Venus atmosphere with the Magellan spacecraft: 1. Experimental description and performance, *Icarus*, *110*, 71–78, doi:10.1006/icar.1994.1107.

Strangeway, R. J. (2004), Plasma waves and electromagnetic radiation at Venus and Mars, *Adv. Space Res.*, *33*, 1956–1967, doi:10.1016/j.asr.2003.08.040.

Wait, J. (1962), *Electromagnetic Waves in Stratified Media*, 372 pp., Pergamon, Oxford, N. Y.

Williams, E. R. (1992), The Schumann resonance: A global tropical thermometer, *Science*, *256*, 1184–1187, doi:10.1126/science.256.5060.1184.

Yang, H., V. P. Pasko, and Y. Yair (2006), Three-dimensional finite difference time domain modeling of the Schumann resonance parameters on Titan, Venus, and Mars, *Radio Sci.*, *41*, RS2S03, doi:10.1029/2005RS003431.

Zimmerman, W. B. J. (2006), *Multiphysics Modelling With Finite Element Methods*, 432 pp., World Sci., London.

K. L. Aplin, Space Science and Technology Department, Rutherford Appleton Laboratory, Chilton, Oxon, OX11 0QX, UK.

C. Béghin, LPCE, CNRS 3A, Avenue de la Recherche Scientifique, 45071 Orléans CEDEX 2, France.

J.-J. Berthelier, M. Hamelin, and F. Simões, CETP, IPSL, CNRS 4, Avenue de Neptune, 94107 Saint Maur, France. (fernando.simoes@cetp.ipsl.fr)

B. P. Besser and K. Schwingenschuh, Space Research Institute, Austrian Academy of Sciences, Schmiedlstrasse 6, 8042 Graz, Austria.

R. Grard and J.-P. Lebreton, Research and Scientific Support Department, ESA-ESTEC, Keplerlaan 1, 2200 AG Noordwijk, Netherlands.

J. J. López-Moreno, Instituto de Astrofisica de Andalucia IAA-CSIC, Camino Bajo de Huetor, 50, 18008 Granada, Spain.

G. J. Molina-Cuberos, Applied Electromagnetic Group, Department of Physics, University of Murcia, Murcia 30100, Spain.

T. Tokano, Institut für Geophysik und Meteorologie, Universität zu Köln, Albertus-Magnus-Platz, 50923 Köln, Germany.